Alzheimer's & Dementia 15 (2019) 1286-1295

Featured Article

In vivo measures of tau burden are associated with atrophy in early Braak stage medial temporal lobe regions in amyloid-negative individuals

Sandhitsu R. Das[a,b,c,d,*], Long Xie[b,e], Laura E. M. Wisse[b,e,c], Nicolas Vergnet[b], Ranjit Ittyerah[b,e], Salena Cui[f], Paul A. Yushkevich[b,d,e], David A. Wolk[a,c,d], for the Alzheimer's Disease Neuroimaging Initiative[1]

[a]*Department of Neurology, University of Pennsylvania, Philadelphia, PA, USA*
[b]*Penn Image Computing and Science Laboratory, University of Pennsylvania, Philadelphia, PA, USA*
[c]*Penn Memory Center, University of Pennsylvania, Philadelphia, PA, USA*
[d]*Penn Alzheimer's Disease Core Center, University of Pennsylvania, Philadelphia, PA, USA*
[e]*Department of Radiology, University of Pennsylvania, Philadelphia, PA, USA*
[f]*Jefferson University, Philadelphia, PA, USA*

Abstract

Introduction: It is unclear the degree to which tau pathology in the medial temporal lobe (MTL) measured by ^{18}F-flortaucipir positron emission tomography relates to MTL subregional atrophy and whether this relationship differs between amyloid-β–positive and amyloid-β–negative individuals.

Methods: We analyzed correlation of MTL ^{18}F-flortaucipir uptake with MTL subregional atrophy measured with high-resolution magnetic resonance imaging in a region of interest and regional thickness analysis and determined the relationship between memory performance and positron emission tomography and magnetic resonance imaging measures.

Results: Both groups showed strong correlations between ^{18}F-flortaucipir uptake and atrophy, with similar spatial patterns. Effects in the rhinal cortex recapitulated Braak staging. Correlations of memory recall with atrophy and tracer uptake were observed.

Discussion: Correlation patterns between tau burden and atrophy in the amyloid-β–negative group mimicking early Braak stages suggests that ^{18}F-flortaucipir is sensitive to tau pathology in primary age-related tauopathy. Correlations of imaging measures with memory performance indicate that this pathology is associated with poorer cognition.

Keywords: Tau PET; Atrophy; AV1451; ^{18}F-flortaucipir; Amyloid negative; Amyloid positive; Volume; Medial temporal lobe; Subregion; Subfield; Braak stages; Logical memory

1. Introduction

Alzheimer's disease (AD) is defined by the presence of two core pathologic species, amyloid plaques, and neurofibrillary tangles (NFTs) composed of the proteins amyloid-β and tau, respectively. NFTs are thought to be more directly related to neuronal loss and synaptic dysfunction and, thus, to the cognitive symptoms of the disease relative to amyloid plaques [1,2]. Positron emission tomography (PET) ligands now exist that allow for in vivo visualization of both amyloid plaques and tangles, and these, along with cerebrospinal

[1]Data used in preparation of this article were obtained from the Alzheimer's Disease Neuroimaging Initiative (ADNI) database (adni.loni.usc.edu). As such, the investigators within the ADNI contributed to the design and implementation of ADNI and/or provided data but did not participate in analysis or writing of this report. A complete listing of ADNI investigators can be found at: http://adni.loni.usc.edu/wp-content/uploads/how_to_apply/ADNI_Acknowledgement_List.pdf.

*Corresponding author. Tel.: 215-746-7224 ; Fax: 215-349-8426.
E-mail address: sudas@seas.upenn.edu

https://doi.org/10.1016/j.jalz.2019.05.009

fluid measures of amyloid-β and phosphorylated tau, are now being used to define AD in research settings [3].

Braak and Braak [4] described six stages of NFT spread that begins within the medial temporal lobe (MTL), specifically in a region which they referred to as transentorhinal cortex, which largely coincides with Brodmann area 35 (BA35) and represents the medial portion of the perirhinal cortex. From the transentorhinal cortex (Braak stage I), NFTs spread medially in the entorhinal cortex (ERC; Braak stage II) followed by the CA1 subfield of the hippocampus (Braak stage II/III). Eventually, NFTs extend outside of the MTL to heteromodal association areas and then throughout much of the cortex (Braak IV-VI). Notably, NFTs appear to develop and generally follow this topographic pattern both in the presence or absence of amyloid-β pathology, but their spread is more aggressive when there is concomitant amyloid-β pathology [5]. Conversely, NFT pathology in the absence of cerebral amyloid was recently termed primary age-related tauopathy (PART) [6]. By definition, PART includes individuals who are Braak stage $\leq$ IV and with amyloid plaque burden consistent with Consortium to Establish a Registry for Alzheimer's Disease (CERAD) score of 0 ("Definite" PART) or 1 ("Probable").

It remains uncertain whether current tau tracers are sensitive to PART [7–9]. Furthermore, it is not clear the degree to which MTL measures of tau relate to atrophy within specific MTL subregions in both amyloid-β–positive (A+) and amyloid-β–negative (A−) individuals and whether these are consistent with Braak staging. If this is the case in those without cerebral amyloid, this would provide convergent validity to the sensitivity of a given tau tracer to PART.

The present study leverages the multisite acquisition of amyloid (^{18}F-florbetapir or ^{18}F-florbetaben) and tau (^{18}F-flortaucipir) PET and high-resolution T2-weighted magnetic resonance imaging (MRI; 0.4 × 0.4 × 2.0 mm^3) specifically prescribed for MTL subregional segmentation, collected as part of the Alzheimer's Disease Neuroimaging Initiative (ADNI). ^{18}F-Flortaucipir has demonstrated consistent correlation with local brain atrophy in patients across the AD continuum and binding to the paired helical filamentous tau that makes up the NFTs associated with AD in postmortem studies [7,9–11] Although PET lacks the resolution for measuring tau burden within specific MTL subregions, we will use a summary measure of MTL cortex uptake and relate it to structural changes in these more granular regions as measured from MRI. In the largely cognitively normal and prodromal AD cohort studied here, we predict strongest correlations between structural changes in the earliest Braak stage regions (BA35, ERC, CA1) with the summary measure of MTL cortex ^{18}F-flortaucipir uptake in both A+ and A− individuals.

2. Methods

2.1. Participants

Data used in this study were obtained from the ADNI database. The study cohort consisted of 185 participants; 113 labeled as A− and 72 labeled as A+ based on their amyloid-PET scans. Amyloid-β status (A+ vs. A−) was determined from participants' latest available ^{18}F-florbetapir (N = 183) or ^{18}F-florbetaben (N = 2) scans using a standardized uptake value ratio (SUVR) threshold of $\geq$1.11 for ^{18}F-florbetapir or 1.08 for ^{18}F-florbetaben computed from a well-established composite region of interest (ROI) [12]. Quantiles of the interval between MRI and PET scans in days were ("+" means PET earlier, "−"means MRI earlier): median = −5, 10% = −707, 25% = −41, 75% = 1, 90% = 8, range −1159 to 692. We utilized SUVR data made available by ADNI based on the postprocessing steps described at http://adni.loni.usc.edu/methods/pet-analysis-method/pet-analysis/. We chose the most recent amyloid-PET scan, rather than, in a few cases, the closest one to the MRI, reducing the possibility of some participants accumulating amyloid and crossing the threshold to A+ after the MRI.

A summary of participants' demographic information and psychometric measures are reported in Table 1.

2.2. Image acquisition

A high-resolution T2-weighted structural MRI specifically optimized for imaging the MTL (in-plane resolution

Table 1
Participants characteristics

Group (N)	A− CN (68)	A− MCI (30)	A+ CN (41)	A+ MCI (30)	A+ dementia (16)
Age (years)	69.52 (5.86)	70.82 (5.87)	72.58 (5.87)	71.86 (7.52)	70.48 (8.74)
Education (years)	16.57 (2.42)	16.17 (3.34)	17.05 (2.36)	16.13 (2.75)	15.56 (2.78)
Sex (M/F)	36/32	13/17	22/19	13/17	10/6
Logical Memory	14.49 (3.46)	10.33 (4.11)	14.8 (3.22)	7.03 (5.28)	2.19 (3.64)
MMSE	29.21 (1.19)	28.63 (1.45)	28.78 (1.51)	27.2 (2.17)	21.33 (4.98)
APOE status (E4 carrier %)	17.6%	13.3%	43.9%	60%	50%

NOTE. Mean and standard deviation are shown. The Logical Memory Test score was obtained from the NEUROBAT_LDELTOTAL variable in ADNI.

Abbreviations: A+, amyloid-β positive; A−, amyloid-β negative; ADNI, Alzheimer's Disease Neuroimaging Initiative; *APOE*, apolipoprotein E; CN, controls; MCI, mild cognitive impairment; MMSE, Mini-Mental State Examination.

of 0.4 × 0.4 mm^2, slice thickness 2.0 mm) was used for making subregional volume and thickness measurements. The high in-plane resolution makes it possible to visualize the internal structure of the hippocampus and to separate MTL cortical gray matter from dura mater, making these scans ideal for subregional MTL morphometry. ^{18}F-flortaucipir PET scans acquired closest in time to the structural MRI were used for estimating tau burden in MTL (the following were quantiles of the interval between MRI and PET scans in days: median = −14, 10% = −565, 25% = −64, 75% = 0, 90% = 1.6, range −1377 to 521). Tau PET imaging consisted of a continuous 30-minute brain scan (6 frames of 5-minute duration) 75 minutes following approximately 10 mCi of ^{18}F-flortaucipir injection. ^{18}F-flortaucipir PET images were downloaded from the ADNI data archive in the most fully postprocessed format with the image description "Coreg, Avg, Std Img and Vox Siz, Uniform Resolution."

2.3. Image processing

T2-weighted MRI was automatically segmented using the multi-atlas labeling technique implemented in the ASHS software [13], providing labels for the hippocampal subfields CA1, CA2, CA3, dentate gyrus (DG), and subiculum (SUB) and regions of the extrahippocampal MTL cortex including entorhinal cortex, perirhinal cortex, subdivided into BA35 and BA36, and parahippocampal cortex (PHC). These segmentations were used to generate volumetric measurements of the hippocampal subfields. In addition, a multi-template shape analysis technique that explicitly accounts for the existence of multiple discrete variants of the collateral sulcus [14] was applied to the segmentations, resulting in point-wise correspondence maps of the MTL subregions across all subjects in an MTL-specific template space. These maps are then used to generate summary thickness measurements for the extrahippocampal cortical ROIs, and to conduct regional thickness analysis within the ribbon that includes the aforementioned MTL cortical subregions in addition to hippocampal subfields CA and subiculum. All MRI images, automatic MTL segmentations, and quality of coregistration between structural MRI and PET images were visually checked for acceptable quality. 37 data sets were excluded from 222 participants with MRI and both PET scans.

The postprocessed ^{18}F-flortaucipir PET images were generated by averaging coregistered individual frames, re-oriented in a standardized image space such that the anterior-posterior axis of the subject is parallel to the AC-PC line, followed by scanner-specific filtering to generate an image with a uniform isotropic resolution of 8-mm full width half maximum. More details about the preprocessing used is described at http://adni.loni.usc.edu/methods/pet-analysis-method/pet-analysis/. Postprocessed PET images were then registered to subject's T1-weighted structural MRI using ANTs [15]. The following ANTs parameters were used: Metric: Mattes mutual information (weight = 1, number of bins = 32), Transformation model: Rigid (gradient step = .2), Smoothing levels = 4 × 2 × 0, Shrink factor = 4 × 2 × 1. The MRI scan was parcellated into cerebellar, cortical, and subcortical ROIs using a multi-atlas segmentation method [16]. The atlas set and the resulting segments are described in the study by Landman and Warfield [17]. Mean PET tracer uptake in the cerebellar gray matter was used as a reference region, and a SUVR map was generated for each participant. A summary measure of MTL cortex tau burden was computed as the average ^{18}F-flortaucipir SUVR in a composite MTL cortical ROI consisting of the BA35 region of the perirhinal cortex and ERC. We did not include the hippocampus in this summary measure, given its proximity to the choroid plexus and known off-target binding of ^{18}F-flortaucipir [18].

2.4. Statistical analysis

Partial linear correlation was used to assess the relationship between MTL cortex tau burden and subregional atrophy in A+ and A− participants separately. Volumes of hippocampal subfields (CA1, CA2, CA3, DG, and SUB) and thickness of extrahippocampal cortices (BA35, BA36, ERC, and PHC), averaged over both hemispheres, were correlated with MTL cortex tau burden. Age, sex, and time between MRI and ^{18}F-flortaucipir PET scan were used as nuisance covariates in all analyses. In addition, intracranial volume was a nuisance covariate in analyses involving hippocampal subfield volumes. Bonferroni correction was used for multiple comparisons correction. An additional interaction analysis was carried out in the entire cohort where an interaction term between composite amyloid-PET SUVR and ^{18}F-flortaucipir MTL cortex was used as a predictor of atrophy in the linear model. In addition to these ROI analyses, regional thickness analysis was performed in the MTL-specific template. The summary measure of MTL cortex tau burden was correlated with local thickness using the same linear correlation framework as used in ROI analysis. To account for multiple comparisons, this analysis used cluster-level family-wise error rate correction [19] with clusters defined using an empirical threshold of uncorrected $P < .05$. Permutation testing with 1000 permutations (with clusters pooled between the left and right hemispheres) was used to assign a corrected P value to each cluster.

In addition to the multimodality imaging correlations, atrophy and tau measures were also correlated with delayed recall on the Wechsler Memory Scale–Revised Logical Memory Test [20] in a partial correlation framework. Cutoffs for this measure determine mild cognitive impairment status in ADNI. For this analysis, age, years of education, and time between cognitive testing and imaging were used as nuisance covariates. In addition, intracranial volume was used as a covariate when volumetric

atrophy measure was used. As a supplementary analysis, these correlations were repeated with the Rey Auditory Verbal Learning Test (AVLT; AVLT 30-minute Delayed Recall and AVLT d-prime recognition score) [21].

2.5. Sensitivity analysis

To mitigate against the possibility that individuals with subthreshold levels of amyloid accumulation might be erroneously classified in the A− group, the primary analysis of ^{18}F-flortaucipir uptake versus atrophy correlations was repeated with a lower amyloid threshold of 1.0 to determine group status. For this analysis, two subjects with ^{18}F-florbetaben scans were excluded.

3. Results

3.1. ROI analysis

Results of ROI analysis examining relationship between tau burden measured by ^{18}F-flortaucipir and volume or thickness are presented in the left two columns in Table 2. Broadly, several ROIs showed significant correlations in both the A− and A+ groups. In the A− group, the BA35 and ERC emerged as statistically the most significant, in absolute terms, with CA1 and subiculum also showing significant but less-strong correlations and subiculum not surviving Bonferroni correction. Only PHC and DG did not reach the threshold for statistical significance consistent with these regions having less early NFT pathology based on Braak staging. Scatterplots of BA35 and CA1 data are displayed in Fig. 1. Note that one outlier was removed from the A− group who had much higher ^{18}F-flortaucipir MTL uptake (SUVR = 1.98) and significant atrophy. These effects were not present when the analysis was restricted to only cognitively normal A− individuals, likely due to a limited range of variance for the imaging measurements.

A very similar pattern was observed in the A+ group in which all the regions except for PHC displayed a significant correlation with MTL cortex ^{18}F-flortaucipir uptake. BA35 thickness displayed the strongest correlation, in absolute terms, of the extrahippocampal regions followed by ERC and BA36. In the hippocampus proper, CA1 volume displayed the strongest correlation with MTL cortex ^{18}F-flortaucipir uptake followed by the DG and subiculum. In general, partial correlations were of somewhat higher magnitude in the A+ than A−group, as well as having a greater range of SUVR values for MTL cortex uptake (Fig. 1).

Table 2
Partial correlations of MTL subregional atrophy with MTL cortex tau burden (left) and logical memory scores (right) in the A− and A+ groups

Group	Partial correlation with summary MTL cortex tau burden		Partial correlation with logical memory scores	
ROI	*P* value	Partial *r*	*P* value	Partial *r*
A− group				
BA35	.0001*	-0.38	.003†	0.34
BA36	.022	-0.24	.03	0.26
ERC	9.00E-05*	-0.39	.001*	0.36
PHC	.05	-0.20	.55	0.10
CA1	.002†	-0.31	.35	0.15
DG	.06	-0.20	.68	0.12
SUB	.01‡	-0.26	.40	0.13
MTL Tau			.005†	-0.28
A+ group				
BA35	1.50E-05*	-0.45	7.5E-08*	0.55
BA36	.004†	-0.31	.002†	0.33
ERC	.0006†	-0.36	.0004†	0.38
PHC	.04	-0.22	.02	0.26
CA1	1.94E-05*	-0.45	4.7E-08*	0.56
DG	6.11E-05*	-0.43	1.3E-05†	0.46
SUB	.001†	-0.35	9.8E-05†	0.41
MTL tau			3.0E-09*	-0.59

NOTE. The last row of each table also shows correlation between MTL cortex tau burden and logical memory. Covariates include time intervals between all pairs of measures included in a given analysis, age, sex, intracranial volume (for volumes but not for thickness), and years of education (for memory correlations). Bonferroni-corrected *P* values are indicated as $^{*}P < .001$, $^{\dagger}P < .05$, $^{\ddagger}P < .1$

Abbreviations: BA35, Brodmann area 35; BA36, Brodmann area 36; ERC, entorhinal cortex; PHC, parahippocampal cortex; DG, dentate gyrus; SUB, subiculum; MTL, medial temporal lobe.

3.2. Supplementary analysis

The partial correlation analyses were repeated to rule out effects of certain confounding factors. These were (1) *Sensitivity analysis:* When participants were assigned to A+ or A− groups based on a lower and more conservative ^{18}F-florbetapir composite threshold of 1.0, the results remained largely similar. These data are included as supplementary material (Supplementary Table 1); (2) *Interaction analysis:* When an interaction term between amyloid and tau tracer uptake was added to the partial correlation analysis, no significant interaction was found (Supplementary Table 2); (3) *Provenance covariate*: When site of acquisition was added as a covariate, it did not have a significant effect; and (4) *Apolipoprotein E (APOE) status*: Adding *APOE* e4 carrier status as a covariate did not have a significant effect. Another secondary analysis examined the correlation of global amyloid tracer uptake with MTL cortex ^{18}F-flortaucipir uptake in both groups, with age as a covariate. Significant correlation was only found in A+ ($P = .001$), not in A− ($P = .6$) group.

3.3. Relationship with memory performance

Delayed recall performance on the Logical Memory Test was significantly correlated with both subregional atrophy and ^{18}F-flortaucipir uptake in both A− and A+ groups. The atrophy correlations were strongest, in absolute terms, in the rhinal cortices. In A−, only BA35 and ERC effects survived multiple comparisons correction (Table 2).

Measures of the AVLT test scores also showed strong correlations with atrophy and ^{18}F-flortaucipir uptake in A+, with BA35 showing the strongest effects in absolute terms

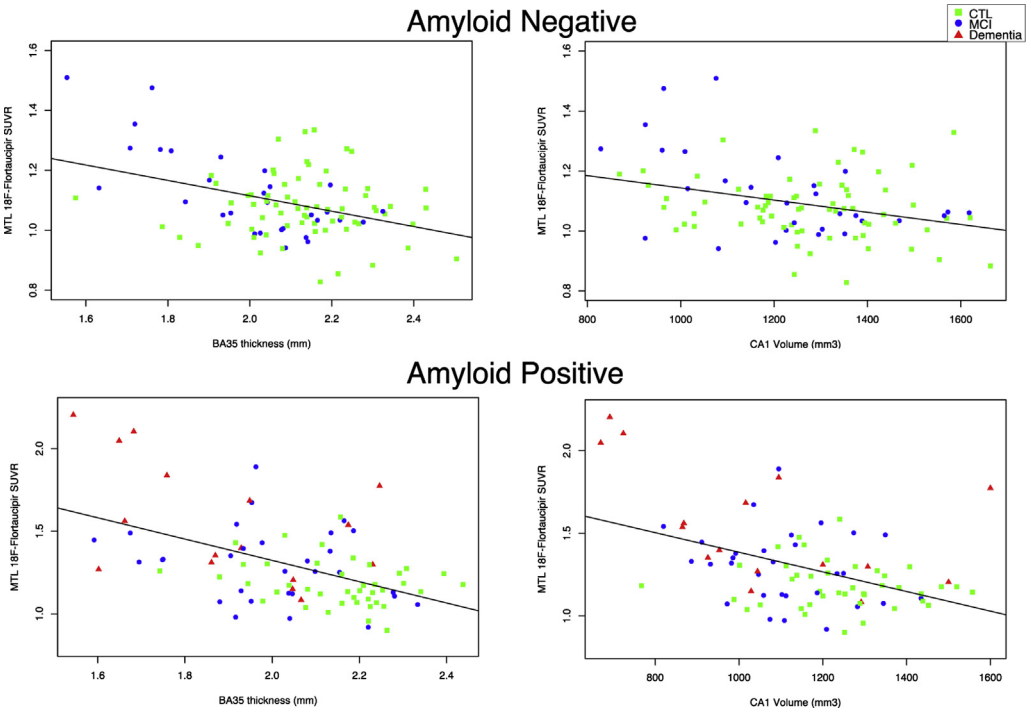

Fig. 1. Scatterplots showing MTL cortex tau burden versus MTL subregional atrophy measures in A+ and A− groups. Abbreviations: A+, amyloid-β positive; A−, amyloid-β negative; BA35, Brodmann area 35; BA36, Brodmann area 36; MTL, medial temporal lobe.

among the cortical regions and CA1 among the hippocampal subfields. Correlations with AVLT scores were weaker in A−. The only significant correlations were found in BA35 and ERC, but these effects did not survive Bonferroni correction (Supplementary Table 3).

3.4. Regional thickness analysis

Regional thickness analysis helps visualize tau-atrophy correlations within the MTL cortical ribbon consisting of the extrahippocampal cortical ROIs and extending into SUB and CA subfields of the hippocampus. In contrast to the ROI analysis, this technique allows for exploration of regional clusters of significant correlations that can extend across subregional boundaries. Fig. 2 recapitulates the results of ROI analysis in the MTL cortex, displaying strong clusters of significant correlation of ^{18}F-flortaucipir uptake with thinning in BA35 and ERC clusters in both groups, regardless of amyloid status. In the hippocampus, significant clusters can be seen straddling CA1 and SUB in the A+ group, with only smaller clusters present in the hippocampus in the A− group.

Fig. 2 also displays the overlap of these significant correlations between the two groups. Remarkably, there is considerable overlap in BA35 and ERC, particularly around the region Braak and Braak referred to as transentorhinal cortex. In the CA1 and subiculum region, although most of the areas of high correlations in A− overlapped with the A+ clusters, they did not reach statistical significance with family-wise error rate correction. There is some tendency for the region of significance in the A− group compared with A+ group to be shifted more toward the CA1/CA2 boundary compared with the A+ group (see red circle in Fig. 2). In both the A+ and A− groups, the maps of the relationship between ^{18}F-flortaucipir uptake and MTL thinning exhibit remarkable symmetry between the left and right hemispheres.

4. Discussion

In this study, we present strong evidence for the in vivo sensitivity of ^{18}F-flortaucipir to tau burden in PART and its linkage to structural changes in the MTL and memory. A defining feature of disease stage in AD is the spread of NFTs in the MTL and beyond, which have come to be described as Braak stages based on the landmark work of Braak and Braak [4]. A relatively stereotyped pattern of involvement within specific regions of the MTL constitutes the first three Braak stages and supports the notion of differential vulnerability of the integrity of these structures to the earliest pathologic changes of AD. Although this pattern of NFT spread is linked to AD, biologically defined by the presence of both amyloid-β plaque and NFT pathology [22,23], Braak and Braak originally described a large number of individuals with minimal or no cerebral amyloid-β who also exhibited NFTs consistent with early Braak stages [24]. Indeed, by the mean age of the present cohort, more than 80% of the individuals in the Braak and Braak cohort were classified as at least Braak stage I or II, regardless of the presence of amyloid-β.

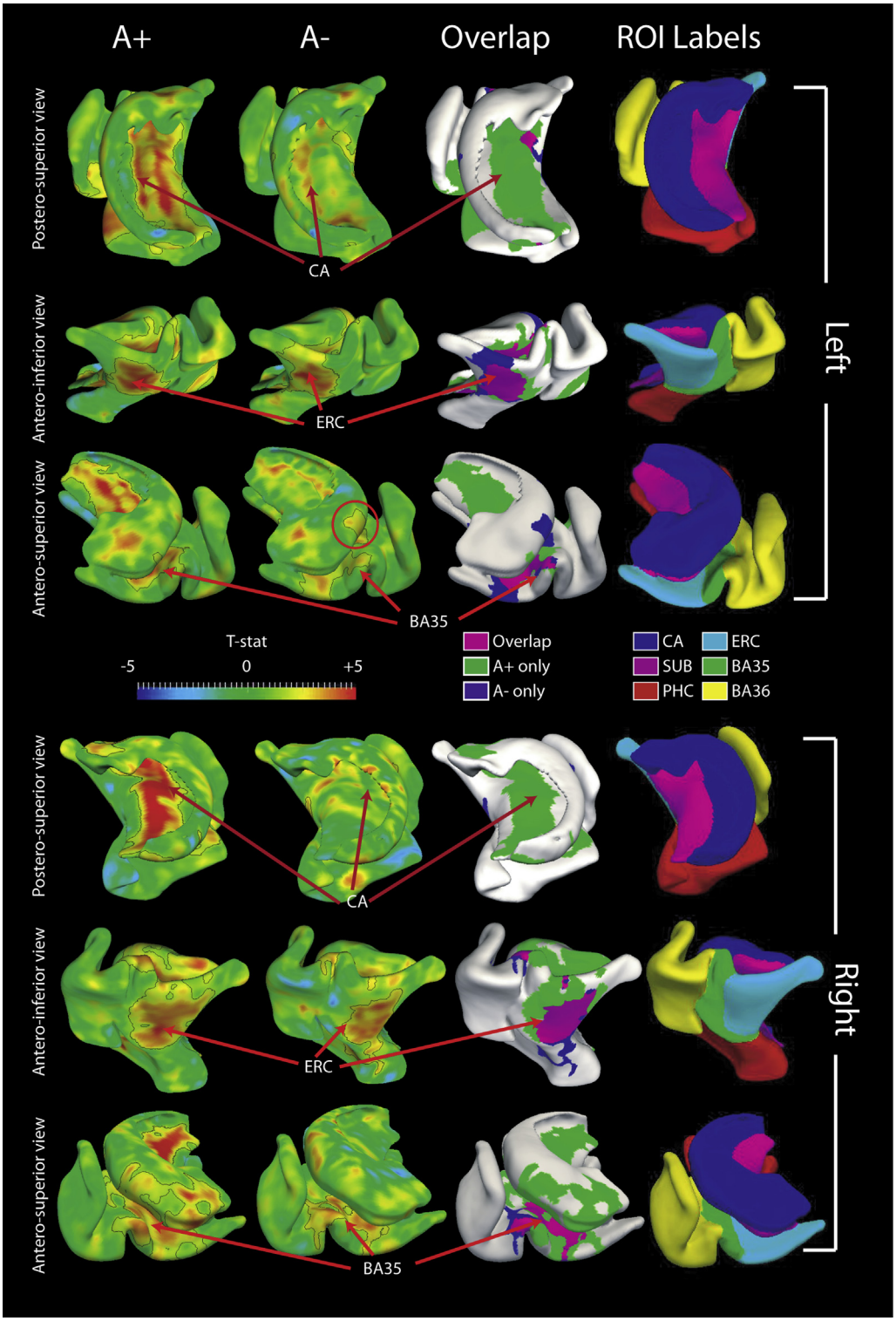

Fig. 2. T-statistic map of partial correlation between tau burden and local thickness in the MTL cortical ribbon, with time between MRI and PET scans and age as covariates. Significant clusters after family-wise error rate correction are circumscribed with black contours. There is considerable overlap between A+ and A− clusters on both sides. However, hippocampal clusters in A− tend to extend farther distally from the subiculum-CA boundary in the body region near the CA1/CA2 boundary, e.g., as indicated by the red circle on the left hemisphere. Abbreviations: A+, amyloid-β positive; A−, amyloid-β negative; BA35, Brodmann area 35; BA36, Brodmann area 36; ERC, entorhinal cortex; PHC, parahippocampal cortex; DG, dentate gyrus; SUB, subiculum; MTL, medial temporal lobe; ROI, region of interest.

These individuals who exhibited NFTs with none to minimal cerebral amyloid-β were more recently given the moniker of PART, a pathological category defined by Braak stage ≤IV and either absent or sparse amyloid plaque burden [6]. Although the clinical implications of PART remain uncertain and may reflect a primary driver of "normal" age-associated decline, some postmortem work has suggested that the degree of NFT pathology in PART is associated with antemortem cognitive decline and hippocampal atrophy [25,26]. Indeed, Crary et al. described progressively lower MMSE scores with higher Braak stage in PART [6].

The present study leveraged advances in in vivo imaging to estimate MTL cortex tau burden with the PET tracer, ^{18}F-flortaucipir [27], and measures of MTL subregional structural integrity with MRI [13]. We examined individuals from ADNI who had both an ^{18}F-flortaucipir tau PET and an amyloid-PET (^{18}F-florbetapir or ^{18}F-florbetaben) scan, as well as a high in-plane resolution T2-weighted scan specifically prescribed for MTL subregional measurement. A number of studies have reported that uptake of ^{18}F-flortaucipir in the MTL cortex correlates with hippocampal, entorhinal, and transentorhinal volume or thickness in A+ individuals ([5,8,11]). Furthermore, we recently demonstrated that BA35 and ERC displayed increased longitudinal thinning in relationship to higher ^{18}F-flortaucipir SUVR in the MTL cortex [28] in A+ individuals, although that study did not find any effects in A−. The current findings provide further support for tau burden in the MTL being disproportionately associated with the regions affected earliest by NFTs based on the pathological literature.

It is less clear the degree to which ^{18}F-flortaucipir is sensitive to the NFTs of PART. Autoradiographic studies have reported binding of ^{18}F-flortaucipir in PART cases that varies based on the degree of maturity of the tangles [7]. In vivo studies have provided mixed results with regard to the degree to which tracer uptake correlates with hippocampal or MTL structural measures in A− individuals with some studies showing a relationship [8] and others not [5,11]. These discrepancies may reflect issues with sample sizes and, thus, power across studies. Finally, some work has supported a relatively specific age-related increase in ^{18}F-flortaucipir uptake in A− individuals consistent with the increased prevalence and degree of NFT deposition in PART [8,29].

The present study utilized an MRI acquisition and automated segmentation approach that allows for more granular measurement of MTL subregions and has been previously shown to be particularly sensitive to early changes in this region associated with AD pathology [13,30]. Furthermore, thickness measurements determined in a pointwise manner across the MTL surface were specifically developed to account for anatomic variants common to the collateral sulcus that impact the lateral boundaries of ERC, BA35, and BA36 [31]. In this context, we observed significant correlation of MTL cortex tracer uptake with cortical thinning most prominently in BA35 and ERC. CA1 and subiculum volume, while weaker in absolute terms than BA35 and ERC, were the regions with strongest correlation within the hippocampus proper.

These findings appear to support the sensitivity of ^{18}F-flortaucipir to PART and suggest that PART has consequences for the integrity of the MTL. Although the relationship described could reflect some kind of nonspecific tracer uptake related to neurodegeneration rather than PART, the fact that the regions most strongly related to this uptake are regions associated with NFTs in Braak stages I and II suggest a relatively specific pattern best explained by NFT pathology. Moreover, the pattern of findings was quite similar to that of the A+ group in which NFTs almost certainly modulate these regional effects. In both groups, the BA35 and ERC are the MTL cortical regions that show the strongest effects in ROI analysis. More impressively, the pink label in Fig. 2 shows remarkable overlapping regions of significant correlation of local thickness and MTL cortex ^{18}F-flortaucipir uptake in the two groups, particularly in the transentorhinal region. This finding is remarkable, as PART and AD-related NFTs are thought to largely display the same spatiotemporal trajectory as demonstrated here. The presence of MTL atrophy in the setting of PART is also consistent with antemortem imaging in pathologically determined cases in which higher Braak stage was associated with greater anterior hippocampal atrophy [26]. One potential difference between the A+ and A− group in the pattern of atrophy was in the hippocampus proper in which the A+ group had stronger correlations. This may reflect the greater range of tracer uptake and tau pathology in A+. Because NFT pathology begins in the MTL cortex and then spreads to the hippocampus, the more restricted range in A− may explain the relatively isolated effects in the MTL cortex in this group. However, it should be noted that some individuals with dementia in the A+ group actually had relatively low tau burden within the range of those in the cognitively normal group. These individuals are more likely to have other concomitant pathologies such as TDP-43 or diminished reserve resulting in their dementia level impairment with less NFTs. In addition, there was a hint that there was relatively greater atrophy associated with MTL SUVR more superiomedially toward the CA1/CA2 boundary in the A− group relative to the greater subicular/CA1 correlation in the A+ group. Although clearly not definitive, this finding is consistent with some recent work suggesting PART is associated with relatively greater CA2 burden than AD-related NFTs [32].

It is worth noting that the fact that the A− group included individuals with mild cognitive impairment is consistent with autopsy studies of PART in which higher Braak stages are associated with poorer cognition [6]. Moreover, the regions that displayed the strongest relationship of atrophy to MTL cortex tracer uptake, BA35 and ERC, in the A− group were the regions correlated with delayed recall performance on the Logical Memory Test, similar to that of the

A+ group. This finding is consistent with autopsy data in which Logical Memory Test performance declines more rapidly in individuals with PART who have higher Braak stages of NFT pathology [25]. Notably, another study did not find a relationship between ERC tau burden and cognitive decline in A− but included only cognitively normal controls [33]. Similarly, the reported correlations were not present when the A− group was limited to cognitively normal individuals in the current data set. It is notable that the correlations of MTL subregional atrophy with logical memory were somewhat stronger in absolute terms than correlations with ^{18}F-flortaucipir uptake in the A− group, which could reflect that contribution of non-tau-related factors also affecting structure and function in the BA35 and ERC. In addition, differences in cerebral blood flow may introduce noise in the tau measures. Cerebral blood flow is also associated with cognitive aging [34,35]. Contrary to prior work in A+ individuals [8], a structural measure, BA35, also correlated as strongly as tracer uptake with memory function, which may be due to the enhanced sensitivity of the more granular measurements used here or potentially greater accuracy in the segmentations. The relationships of AVLT memory scores were similar to those of the Logical Memory Test. The only significant effects, which did not survive Bonferroni correction, in the A− groups were in the BA35 and ERC, the two regions of early NFT pathology. In contrast, the A+ group also showed strong correlations in hippocampal subfield CA1, a region where pathology spreads later in the disease course. Taken together, this shows how the brain-behavior relationships in the MTL follow a similar spatiotemporal trajectory in both A− and A+ groups.

There are a couple of additional caveats and limitations in the present study. One is that the SUVR cutoff for A+ and A− PET scans tends to reflect the sensitivity for Thal Aβ phase of 2 or greater or CERAD neuritic plaque frequency of "greater than sparse" [36,37]. Thus, the A− group may include those with "possible" PART (Thal stage 1 or 2, sparse CERAD plaque frequency) rather than exclusively those with "definite" PART (Thal stage 0, no neuritic plaques). To mitigate against this potential confound and recent work suggesting subthreshold uptake is associated with ^{18}F-flortaucipir uptake and interacts with cerebral amyloid levels in relationship to entorhinal thinning [38,39], we performed a sensitivity analysis where a lower SUVR cutoff of 1.0 was used. This resulted in 15 additional individuals being classified as A+. The results were essentially unchanged with this more conservative cutoff, suggesting that individuals with subthreshold amyloid burden did not drive the effects in the A− group. Notably, a direct correlation between global amyloid tracer uptake and MTL cortex tau tracer uptake was only present in the A+ group, further suggesting that there was not a clear link between subthreshold amyloid and NFTs in the A− group. Nonetheless, we cannot completely rule out the possibility that some in the A− group, even with a stricter SUVR cutoff, would fall in the "possible" PART category, given limitations in the sensitivity of the modality. We also found that *APOE* e4 carrier status, which also may influence relationships between tau and amyloid with MTL atrophy, did not impact findings when included as a covariate. However, as expected, the proportion of e4 carriers was lower in the A− group.

It is also possible that the generally stronger correlations between our MTL cortex summary measure of ^{18}F-flortaucipir uptake and extrahippocampal regions rather than hippocampus reflects the fact that the summary ROI did not include the latter region. This choice was made to avoid the off-target uptake in the choroid plexus, which can confound hippocampal measurements. We also note that the limited spatial resolution of PET introduces some amount of signal mixing from neighboring regions even in the summary MTL cortex measure.

In conclusion, the current findings support the notion that ^{18}F-flortaucipir is sensitive to the tau pathology associated with aging, i.e., PART, and that the degree of this pathology results in measurable atrophy in early Braak regions with consequences to cognitive function. As such, one can track this potential contributor to age-related cognitive decline and differentiate from that driven by preclinical AD with multimodal imaging. Finally, this work also supports the notion that structural measurements of regions affected by early NFT pathology may serve as sensitive surrogates of tau-mediated neurodegeneration regardless of amyloid status.

Acknowledgments

Data collection and sharing for this project was funded by the Alzheimer's Disease Neuroimaging Initiative (ADNI) (National Institutes of Health Grant U01 AG024904) and DOD ADNI (Department of Defense award number W81XWH-12-2-0012). ADNI is funded by the National Institute on Aging and the National Institute of Biomedical Imaging and Bioengineering and through generous contributions from the following: AbbVie; Alzheimer's Association; Alzheimer's Drug Discovery Foundation; Araclon Biotech; BioClinica, Inc.; Biogen; Bristol-Myers Squibb Company; CereSpir, Inc.; Cogstate; Eisai Inc.; Elan Pharmaceuticals, Inc.; Eli Lilly and Company; EuroImmun; F.Hoffmann-La Roche Ltd and its affiliated company Genentech, Inc.; Fujirebio; GE Healthcare; IXICO Ltd.; Janssen Alzheimer Immunotherapy Research & Development, LLC.; Johnson & Johnson Pharmaceutical Research & Development LLC.; Lumosity; Lundbeck; Merck & Co., Inc.; Meso Scale Diagnostics, LLC.; NeuroRx Research; Neurotrack Technologies; Novartis Pharmaceuticals Corporation; Pfizer Inc.; Piramal Imaging; Servier; Takeda Pharmaceutical Company; and Transition Therapeutics. The Canadian Institutes of Health Research is providing funds to support ADNI clinical sites in Canada. Private sector contributions are facilitated by the Foundation for the National Institutes of

Health (www.fnih.org). The grantee organization is the Northern California Institute for Research and Education, and the study is coordinated by the Alzheimer's Therapeutic Research Institute at the University of Southern California. ADNI data are disseminated by the Laboratory for Neuro Imaging at the University of Southern California.
This work was also supported by National Institutes of Health grant numbers R01 DC014296, R21 AG051987, R01 AG037376, R01 AG056014, R01 EB017255, R03 EB016923, and R01 AG055005 and the donors of Alzheimer's Disease Research, a program of the BrightFocus Foundation (L.E.M.W.).

Supplementary Data

Supplementary data related to this article can be found at https://doi.org/10.1016/j.jalz.2019.05.009.

RESEARCH IN CONTEXT

1. Systematic review: The authors reviewed the literature using traditional resources, such as PubMed and Google Scholar, and from recent conference presentations. There has been considerable work on relating in vivo tau PET measures with atrophy in structural magnetic resonance imaging. These studies have been appropriately cited.
2. Interpretation: Evidence for strong correlations between medial temporal lobe subregional atrophy and the Logical Memory Test performance with ^{18}F-flortaucipir uptake that follow a strikingly similar topographic pattern in both amyloid-negative and amyloid-positive individuals recapitulating early Braak stages suggests that this tracer is sensitive to tau pathology in primary age-related tauopathy.
3. Future directions: The manuscript opens up possibilities of testing hypotheses examining effects of tau pathology at a more granular level within the medial temporal lobe in primary age-related tauopathy, including relating tau burden with longitudinal atrophy rates in medial temporal lobe subregions, as well as other functional imaging markers.

References

[1] Bobinski M, Wegiel J, Tarnawski M, Bobinski M, Reisberg B, De Leon MJ, et al. Relationships between regional and neuronal loss and neurofibrillary changes in the hippocampal formation and duration and severity of Alzheimer disease. J Neuropathol Exp Neurol 1997; 56:414–20.
[2] Fukutani Y, Kobayashi K, Nakamura I, Watanabe K, Isaki K, Cairns NJ. Neurons, intracellular and extracellular neurofibrillary tangles in subdivisions of the hippocampal cortex in normal ageing and Alzheimer's disease. Neurosci Lett 1995;200:57–60.
[3] Jack CR, Bennett DA, Blennow K, Carrillo MC, Dunn B, Haeberlein SB, et al. NIA-AA Research Framework: Toward a biological definition of Alzheimer's disease. Alzheimers Dement 2018; 14:535–62.
[4] Braak H, Braak E. Neuropathological stageing of Alzheimer-related changes. Acta Neuropathol 1991;82:239–59.
[5] Wang L, Benzinger TL, Su Y, Christensen J, Friedrichsen K, Aldea P, et al. Evaluation of Tau Imaging in Staging Alzheimer Disease and Revealing Interactions Between β-Amyloid and Tauopathy. JAMA Neurol 2016;73:1070–7.
[6] Crary JF, Trojanowski JQ, Schneider JA, Abisambra JF, Abner EL, Alafuzoff I, et al. Primary age-related tauopathy (PART): a common pathology associated with human aging. Acta Neuropathol 2014; 128:755–66.
[7] Lowe VJ, Curran G, Fang P, Liesinger AM, Josephs KA, Parisi JE, et al. An autoradiographic evaluation of AV-1451 Tau PET in dementia. Acta Neuropathol Commun 2016;4:58.
[8] Maass A, Lockhart SN, Harrison TM, Bell RK, Mellinger T, Swinnerton K, et al. Entorhinal tau pathology, episodic memory decline, and neurodegeneration in aging. J Neurosci 2018;38:530–43.
[9] Marquié M, Normandin MD, Vanderburg CR, Costantino IM, Bien EA, Rycyna LG, et al. Validating novel tau positron emission tomography tracer [F-18]-AV-1451 (T807) on postmortem brain tissue. Ann Neurol 2015;78:787–800.
[10] Bejanin A, Schonhaut DR, La Joie R, Kramer JH, Baker SL, Sosa N, et al. Tau pathology and neurodegeneration contribute to cognitive impairment in Alzheimer's disease. Brain 2017;140:3286–300.
[11] Das SR, Xie L, Wisse LEM, Ittyerah R, Tustison NJ, Dickerson BC, et al. Alzheimer's Disease Neuroimaging Initiative. Longitudinal and cross-sectional structural magnetic resonance imaging correlates of AV-1451 uptake. Neurobiol Aging 2018;66:49–58.
[12] Landau SM, Breault C, Joshi AD, Pontecorvo M, Mathis CA, Jagust WJ, et al. Alzheimer's Disease Neuroimaging Initiative. Amyloid-β imaging with Pittsburgh compound B and florbetapir: comparing radiotracers and quantification methods. J Nucl Med 2013;54:70–7.
[13] Yushkevich PA, Pluta JB, Wang H, Xie L, Ding S-L, Gertje EC, et al. Automated volumetry and regional thickness analysis of hippocampal subfields and medial temporal cortical structures in mild cognitive impairment. Hum Brain Mapp 2015;36(1):258–87.
[14] Ding S-L, Van Hoesen GW. Borders, extent, and topography of human perirhinal cortex as revealed using multiple modern neuroanatomical and pathological markers. Hum Brain Mapp 2010;31:1359–79.
[15] Avants BB, Epstein CL, Gee JC. (12AD). Symmetric shape averaging in the diffeomorphic space. Biomedical Imaging: From Nano to Macro, 2007 2007. 4th IEEE International Symposium on ISBI, 2007. p. 636–9, https://doi.org/10.1109/ISBI.2007.356932.
[16] Wang H, Suh JW, Das S, Pluta J, Altinay M, Yushkevich P. Regression-based label fusion for multi-atlas segmentation. Conf Comput Vis Pattern Recognit Workshops 2011;20:1113–20.
[17] Landman B, Warfield S. MICCAI 2012 workshop on multi-atlas labeling. In: Medical image computing and computer assisted intervention conference; 2012.
[18] Lee CM, Jacobs HIL, Marquié M, Becker JA, Andrea NV, Jin DS, et al. 18F-flortaucipir binding in choroid plexus: related to race and hippocampus signal. J Alzheimers Dis 2018;62:1691–702.
[19] Hayasaka S, Nichols TE. Validating cluster size inference: Random field and permutation methods. NeuroImage 2003;20:2343–56.
[20] Wechsler D. Wechsler Memory Scale: Revised Manual 1987. San Antonio, TX: Psychological Corporation; 1987.

[21] Rey A. The Clinical Examination in Psychology 1964. Paris: University Presses of France; 1964.
[22] Hyman BT, Phelps CH, Beach TG, Bigio EH, Cairns NJ, Carrillo MC, et al. National Institute on Aging–Alzheimer's Association guidelines for the neuropathologic assessment of Alzheimer's disease. Alzheimers Dement 2012;8:1–13.
[23] Montine TJ, Phelps CH, Beach TG, Bigio EH, Cairns NJ, Dickson DW, et al. Alzheimer's Association. National Institute on Aging-Alzheimer's Association guidelines for the neuropathologic assessment of Alzheimer's disease: a practical approach. Acta Neuropathol 2012;123:1–11.
[24] Braak H, Braak E. Frequency of stages of Alzheimer-related lesions in different age categories. Neurobiol Aging 1997;18:351–7.
[25] Jefferson-George KS, Wolk DA, Lee EB, McMillan CT. Cognitive decline associated with pathological burden in primary age-related tauopathy. Alzheimers Dement 2017;13:1048–53.
[26] Josephs KA, Murray ME, Tosakulwong N, Whitwell JL, Knopman DS, Machulda MM, et al. Tau aggregation influences cognition and hippocampal atrophy in the absence of beta-amyloid: a clinico-imaging-pathological study of primary age-related tauopathy (PART). Acta Neuropathol 2017;133:705–15.
[27] Xia C-F, Arteaga J, Chen G, Gangadharmath U, Gomez LF, Kasi D, et al. [18F]T807, a novel tau positron emission tomography imaging agent for Alzheimer's disease. Alzheimers Dement 2013;9:666–76.
[28] Xie L, Das SR, Wisse LEM, Ittyerah R, Yushkevich PA, Wolk DA. Early Tau Burden Correlates with Higher Rate of Atrophy in Transentorhinal Cortex. J Alzheimers Dis 2018;62:85–92.
[29] Schöll M, Lockhart SN, Schonhaut DR, O'Neil JP, Janabi M, Ossenkoppele R, et al. PET Imaging of Tau Deposition in the Aging Human Brain. Neuron 2016;89:971–82.
[30] Wolk DA, Das SR, Mueller SG, Weiner MW, Yushkevich PA. Medial temporal lobe subregional morphometry using high resolution MRI in Alzheimer's disease. Neurobiol Aging 2017;49:204–13.
[31] Xie L, Pluta JB, Das SR, Wisse LEM, Avants BB, Yushkevich PA, et al. Multi-template analysis of human perirhinal cortex in brain MRI: Explicitly accounting for anatomical variability. NeuroImage 2017;144:183–202.
[32] Jellinger KA. Different patterns of hippocampal tau pathology in Alzheimer's disease and PART. Acta Neuropathol 2018;136:811–3.
[33] Sperling RA, Mormino EC, Schultz AP, Betensky RA, Papp KV, Amariglio RE, et al. The impact of Aβ and tau on prospective cognitive decline in older individuals. Ann Neurol 2018; 85:25395.
[34] Rabin JS, Schultz AP, Hedden T, Viswanathan A, Marshall GA, Kilpatrick E, et al. Interactive Associations of Vascular Risk and β-Amyloid Burden With Cognitive Decline in Clinically Normal Elderly Individuals. JAMA Neurol 2018;75:1124.
[35] Vemuri P, Lesnick TG, Przybelski SA, Knopman DS, Lowe VJ, Graff-Radford J, et al. Age, vascular health, and Alzheimer disease biomarkers in an elderly sample. Ann Neurol 2017;82:706–18.
[36] Clark CM, Pontecorvo MJ, Beach TG, Bedell BJ, Coleman RE, Doraiswamy PM, et al. AV-45-A16 Study Group. Cerebral PET with florbetapir compared with neuropathology at autopsy for detection of neuritic amyloid-β plaques: a prospective cohort study. Lancet Neurol 2012;11:669–78.
[37] Murray ME, Lowe VJ, Graff-Radford NR, Liesinger AM, Cannon A, Przybelski SA, et al. Clinicopathologic and 11 C-Pittsburgh compound B implications of Thal amyloid phase across the Alzheimer's disease spectrum. Brain 2015;138:1370–81.
[38] Knopman DS, Lundt ES, Therneau TM, Vemuri P, Lowe VJ, Kantarci K, et al. Entorhinal cortex tau, amyloid-β, cortical thickness and memory performance in non-demented subjects. Brain 2019; 142:1148–60.
[39] Leal SL, Lockhart SN, Maass A, Bell RK, Jagust WJ. Subthreshold amyloid predicts tau deposition in aging. J Neurosci 2018; 38:4482–9.